Vortex Effects in the Dynamics of Underwater Weapons

Dr P.A. Lyes
BAE Systems, Underwater Weapons Division
Elettra Avenue, Waterlooville, PO7 7XS, UK

Dr A.P. Steer
DERA, Haslar Road, Gosport, PO12 2AG, UK

Abstract

As the control and mobility of submarines are improved to meet the challenges of the 21st-century security environment, so the capabilities of underwater weapons must keep pace with these developments. An underwater weapon is typically propelled by a pump-jet, controlled by an arrangement of movable lifting surfaces and stabilized by fixed fins. The propulsor, fins and control surfaces are situated close together at the tail, and close to the axis of the weapon due to the requirements for weapons to be launched through tubes. The control and propulsion components form a closely coupled hydrodynamic system, in which the rate of fluid flow through the propulsor strongly affects both the propulsion and the control characteristics of the weapon.

Vortices are generated by the cylindrical body and fins of the weapon during manoeuvres. These are intimately linked with the rest of the flow field generated by the vehicle. It is required to assess the degree to which the manoeuvring forces, experienced by the vehicle, are affected by the vortices, and how these are modified by the effect of the propulsor and control systems.

A detailed model of the propulsor has been developed, using stage interfaces to construct a fluid dynamic model of the duct, working rotor and stator, with resolved flows around the blades. This is a significant advance on models which used a momentum source for the effect of the rotor and stator, but did not include the blade flows. These important developments were carefully analysed. It was shown that the CFD method can predict propulsion characteristics.

The modelling of the complete, three-dimensional vehicle with working propulsor, at angles of yaw, enables the matching of CFD models for the vehicle and propulsor, the computation of forces at yaw angles and validation of the vehicle flow through comparison with measured data.

This work was carried out as part of Technology Group 01 of the MoD Corporate Research Programme.

Introduction

At an early stage in the design process, it is desirable to predict the hydrodynamic derivatives as a function of flow rate. The prediction of pressure distributions on the tail components is also desirable, since it would enable the development of control system algorithms to be brought forward with confidence. If surface pressures are predicted with accuracy and high resolution, then a more optimal structural design can be produced, with savings in both cost and weight.

Studies have been carried out[1] to enhance the detailed understanding of underwater vehicle hydrodynamics through the use of advanced computational fluid dynamics (CFD) tools. The first stage of the work was concerned with modelling axisymmetric flow around a bare torpedo body with and without a duct. These calculations were made with a range of grid refinements, turbulence models and solution schemes, and were compared with test measurements to establish the capabilities of the CFD code. The effect of the propulsor was modelled through the use of body force patches within the duct region.

Paper presented at the RTO AVT Symposium on "Advanced Flow Management: Part A – Vortex Flows and High Angle of Attack for Military Vehicles", held in Loen, Norway, 7-11 May 2001, and published in RTO-MP-069(I).

Report Documentation Page

Form Approved
OMB No. 0704-0188

1. REPORT DATE	2. REPORT TYPE	3. DATES COVERED
00 MAR 2003	**N/A**	**-**

4. TITLE AND SUBTITLE	5a. CONTRACT NUMBER
Vortex Effects in the Dynamics of Underwater Weapons	5b. GRANT NUMBER
	5c. PROGRAM ELEMENT NUMBER
6. AUTHOR(S)	5d. PROJECT NUMBER
	5e. TASK NUMBER
	5f. WORK UNIT NUMBER
7. PERFORMING ORGANIZATION NAME(S) AND ADDRESS(ES) **NATO Research and Technology Organisation BP 25, 7 Rue Ancelle, F-92201 Neuilly-Sue-Seine Cedex, France**	8. PERFORMING ORGANIZATION REPORT NUMBER
9. SPONSORING/MONITORING AGENCY NAME(S) AND ADDRESS(ES)	10. SPONSOR/MONITOR'S ACRONYM(S)
	11. SPONSOR/MONITOR'S REPORT NUMBER(S)

12. DISTRIBUTION/AVAILABILITY STATEMENT
Approved for public release, distribution unlimited

13. SUPPLEMENTARY NOTES
Also see: ADM001490, Presented at RTO Applied Vehicle Technology Panel (AVT) Symposium held inLeon, Norway on 7-11 May 2001, The original document contains color images.

14. ABSTRACT

15. SUBJECT TERMS

16. SECURITY CLASSIFICATION OF:			17. LIMITATION OF ABSTRACT	18. NUMBER OF PAGES	19a. NAME OF RESPONSIBLE PERSON
a. REPORT	b. ABSTRACT	c. THIS PAGE			
unclassified	**unclassified**	**unclassified**	**UU**	**12**	

The second stage of the work built upon the first by modelling a three-dimensional representation of the torpedo body with zero incidence and yawed flow impinging upon it. The propulsor model was further improved by representing the three dimensional rotor and stator geometry within the duct of an axisymmetric calculation instead of imposing body forces. This was facilitated through the use of stage interface planes between the blade-rows and the body grid, so that the effect of rotor rotation was properly modelled.

The final stage of the work has drawn together the experience of the initial stages for an analysis of the flow around a fully configured torpedo with duct, tail fins, rotor, stator and rudder. This has been completed for a range of yaw angles, advance ratios, roll rates and rudder deflections.

Grid generation

The overall grid was constructed from a number of grid components that were joined together using general grid interfaces (GGI). These interfaces allow node mismatching across joints, hence the separate grids were generated independently of each other. Another benefit of using the GGI strategy was that a relatively coarse grid could be used for the upstream block and a finer grid used for the detailed tail fin region. A reasonable balance could therefore be made between economy and grid resolution. The upstream grid benefits from having complete rotational symmetry with low levels of cell skewness.

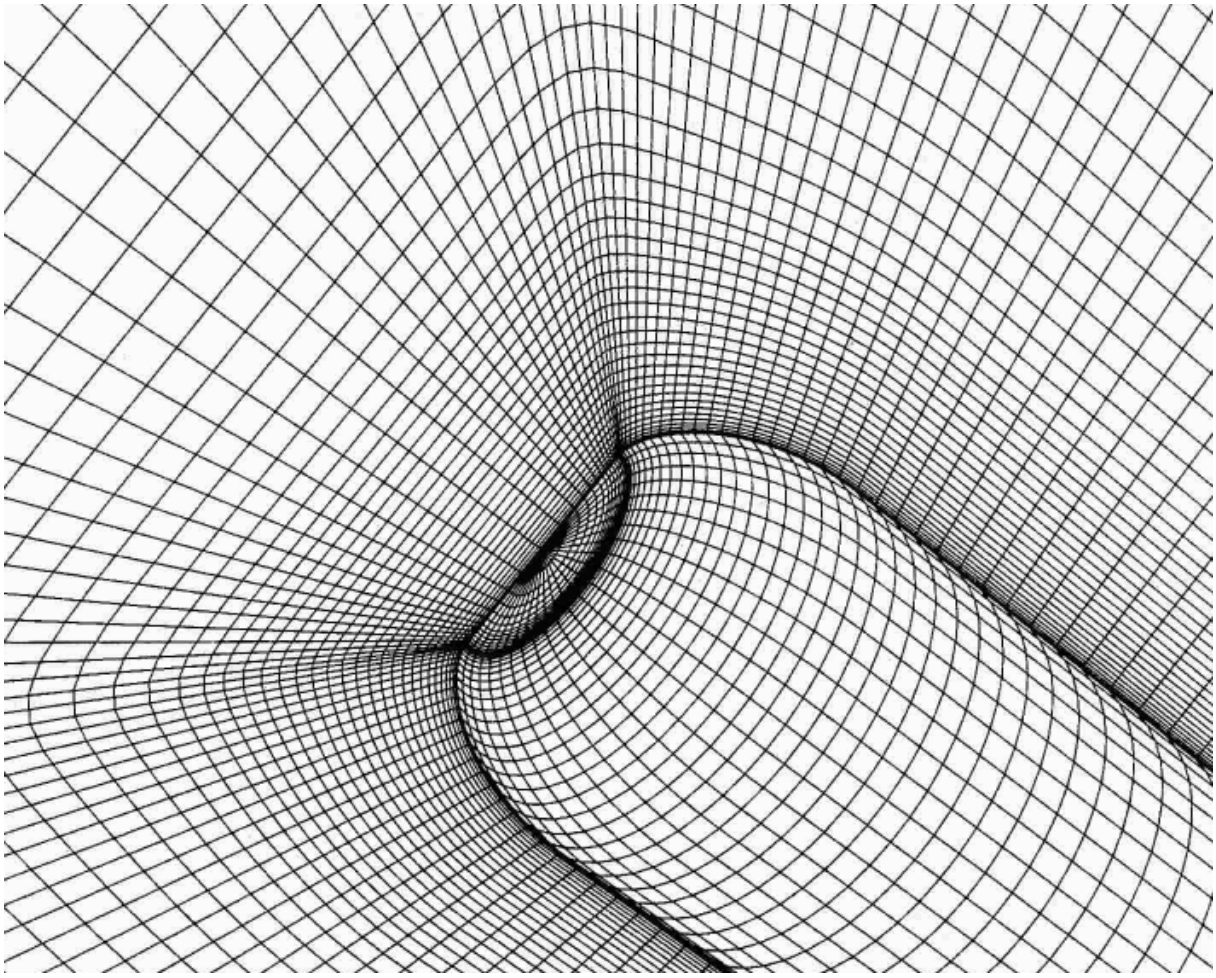

Figure 1: Fore-body grid.

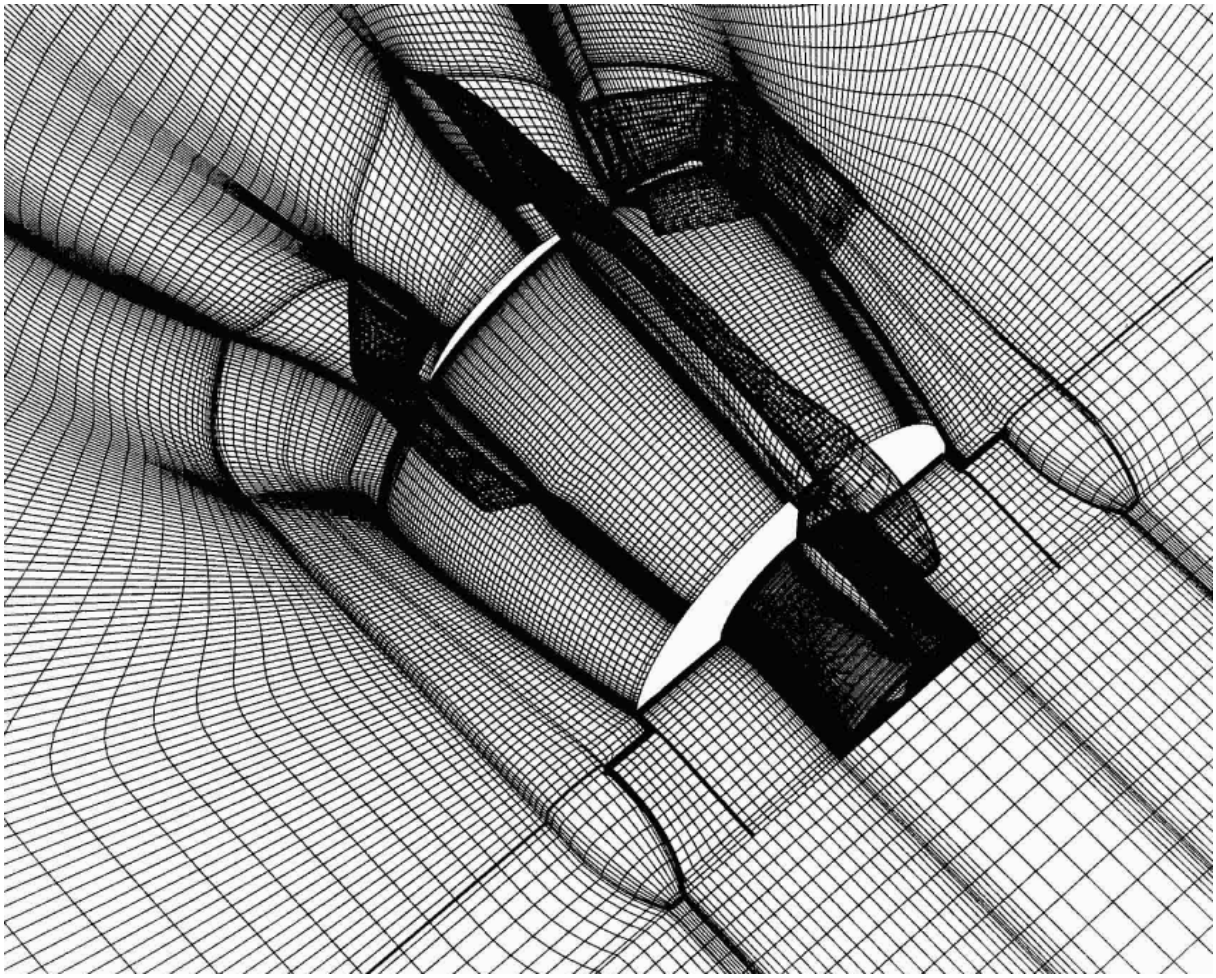

Figure 2: Fin, duct and rudder grid.

Figure 1 shows part of the three-dimensional grid around the fore-body of the vehicle. The grid exploits the inherent rotational symmetry of the geometry and uses a relatively straightforward single block topology. Earlier studies conducted at zero yaw showed that it was important to maintain axial symmetry for the body grid. It was therefore considered important to keep the grid as symmetric and uniform as possible in order to model the effects of body vortices in yawed flows.

The grid generation software was an in-house code, consisting of routines to map a structured grid to each of the fin surfaces, and to generate the volume grid and outer boundaries using a transfinite interpolation method. Advantage was taken of the symmetry of the vehicle to compute only a 90° or 180° sector, aligned along the axis of the flow field, where appropriate. Since the code was specifically developed for this study, the user had control over each node. With some modification further grids could be produced for a range of underwater vehicles with complex tail configurations.

Figure 2 shows the after-body grid comprising body, fin, rudder and duct blocks. The program for generating the rudder grid was structured so that the grid could quickly be re-generated at different deflection angles by changing one number at the top of the code. The grid was first generated around a rudder at zero deflection then the rudder was deflected. A new grid was calculated from a progressive mixture of the new rudder transformation and the original position depending on how far each node is from the rudder and the outer boundaries. The first few layers of cells closest to the rudder surface were rotated with the rudder so that boundary layer grid was not subjected to skew. The GGI strategy was again used to avoid skewed cells between the rudder and fin at high rudder angles, at the leading edge and tip of the rudder.

Commercially available, turbomachinery CFD software, CFX-Tascflow[2], was used to generate the propulsor grid. A multi-block grid was generated around the blades using a pre-defined, O-grid topology template. One blade passage grid was generated for each of the rotor and stator, each containing approximately 100 000 cells. The full-domain grid contained approximately two million cells.

Code convergence and running

The Reynolds Averaged Navier-Stokes equations were solved for turbulent, incompressible flow, at a full-scale Reynolds number of 6 x 10^7. A k-ε turbulence model was used, together with log law functions for near-wall flow. CFX-Tascflow was used to predict the flow around the entire vehicle.

Figure 3 shows the convergence history for a typical run. Root-mean-squared histories for the U, V and W momentum and mass residuals are shown. Local time stepping was applied to accelerate convergence. This strategy implemented time marching at a rate proportional to cell size, and hence promoted more rapid convergence in the far field where cells were large. Since local time-stepping is not conservative, global time marching was used for the final iterations of the solver run. Good convergence was achieved in each of the runs.

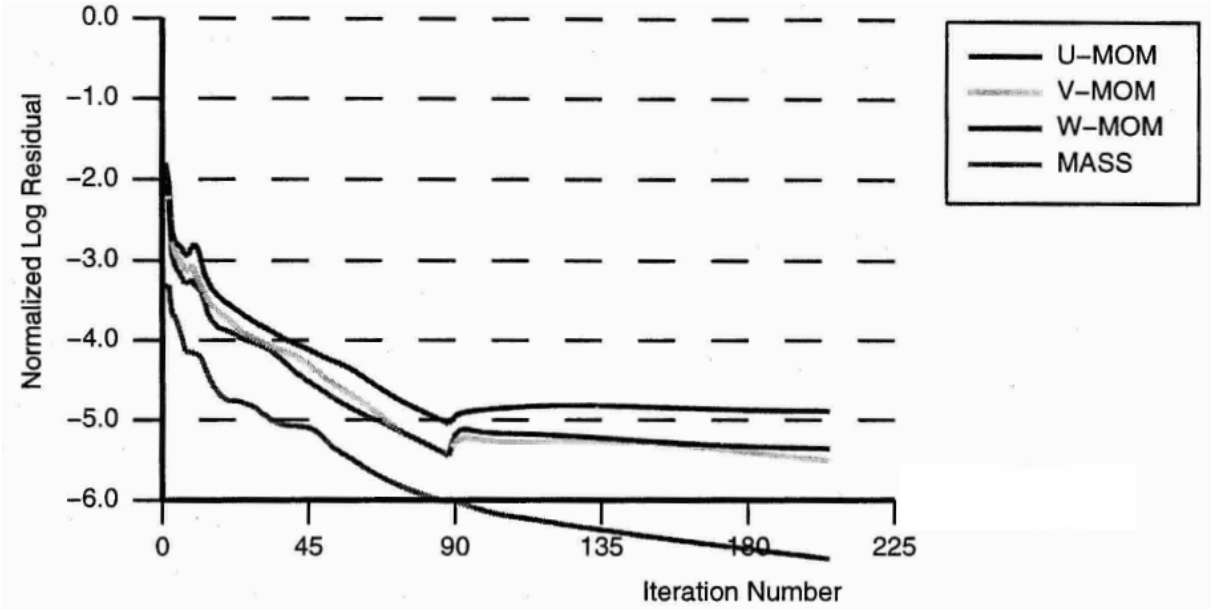

Figure 3: Solver convergence. Root-mean-square residuals.

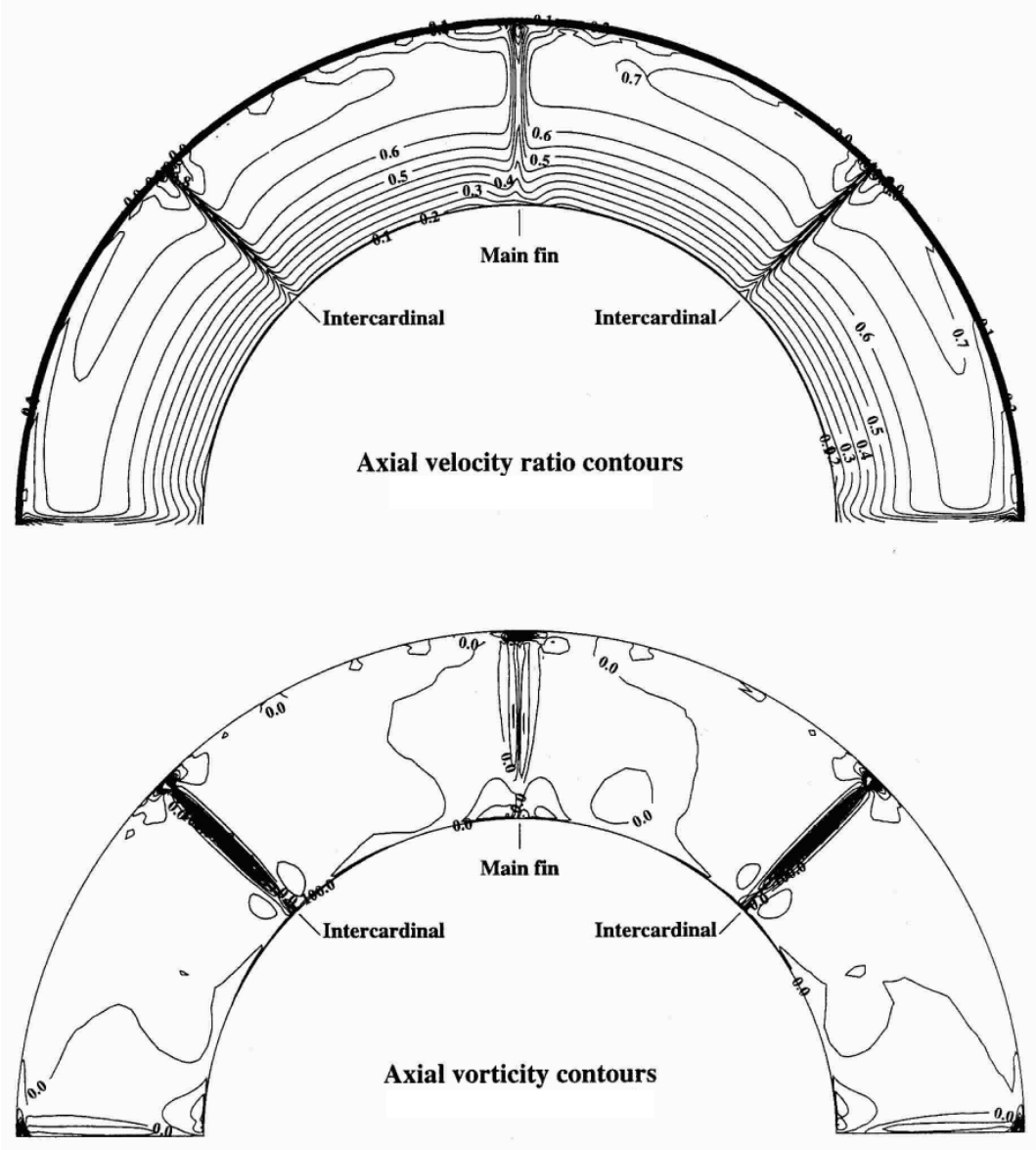

Figure 4: Propulsor in-flow at zero yaw angle.

Flow solutions with zero yaw angle

Calculations have been completed for a 180^{o} sector of grid for the fully appended vehicle operating at zero incidence, with zero rudder deflection. Figure 4 shows contours of axial velocity and vorticity at the inlet to the propulsor. The view is looking upstream. The centrelines of the main-fin and intercardinal fins are indicated.

The main-fin wake is broader than the intercardinal wakes and the flow between the wakes is symmetrically distributed. The intercardinal wakes are narrow with a greater velocity deficit than the main-fin wake. This is because the trailing edge of the intercardinal fin is closer to the inlet plane of the propulsor, hence the wake has less downstream distance to broaden. This is reflected in the vorticity contours that indicate a considerably higher level of vorticity for the intercardinal wakes. The vorticity between the wakes is virtually zero. The bunching of the circumferential contours towards the hub indicate the radial extent of the hub boundary layer.

Flow solutions with rudder deflection

Four computations were conducted to produce predicted propulsor characteristics for a range of advance ratios. The rudder was deflected by 20^o, at zero yaw angle. As the advance ratio decreases, a greater proportion of the flow passes over the rudders and they therefore become more effective at producing a side force.

The effect of the rudder deflection on side force coefficient is shown in figure 5. The experimental measurements were taken in a wind tunnel[3]. Although the predicted coefficients are between ten and fifteen per cent lower than the measurements, the comparison with test is encouraging as the trend of rudder effect with advance ratio is well modelled. The yawing moment coefficient predictions showed a similar trend to those of the side force coefficient shown in figure 5, and to their respective test data curves.

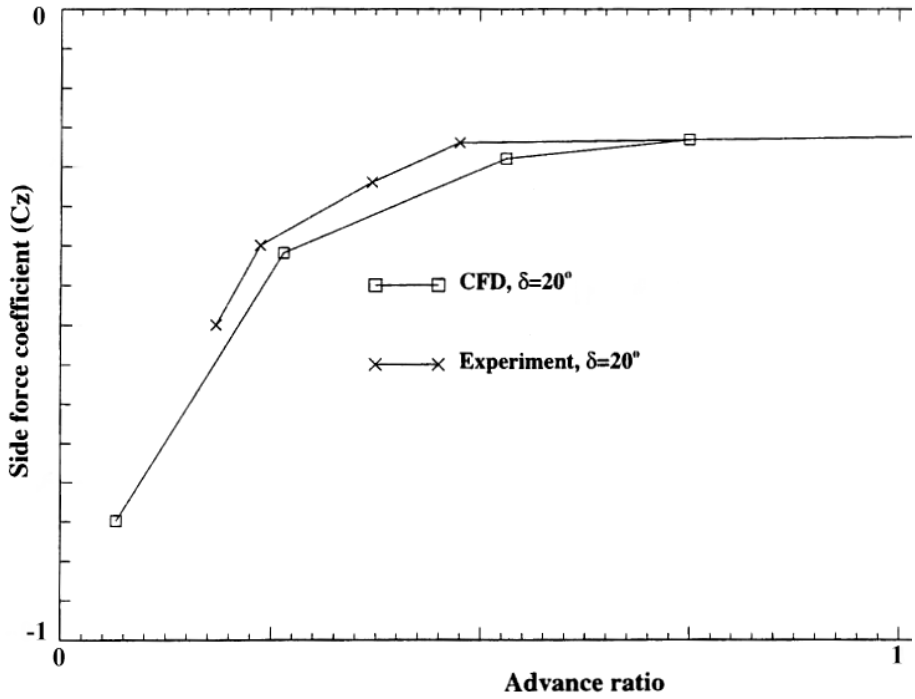

Figure 5: Effect of rudder deflection on side force.

Flow solutions at yaw angle

Yawed flow calculations were completed at 4^o and 10^o of yaw and zero rudder deflection. The outer boundary conditions were modified from the zero yaw angle cases so that one half of the curved boundary became an inflow and the other half an outlet boundary. Figure 6 shows streamlines of the flow solution, with spectrum colour-coding: blue represents low speed, red represents high speed. Wake vortices from the fins are indicated, as is the disturbed flow due to the body vortex, but vortices in the propulsor inflow are not visible at this resolution.

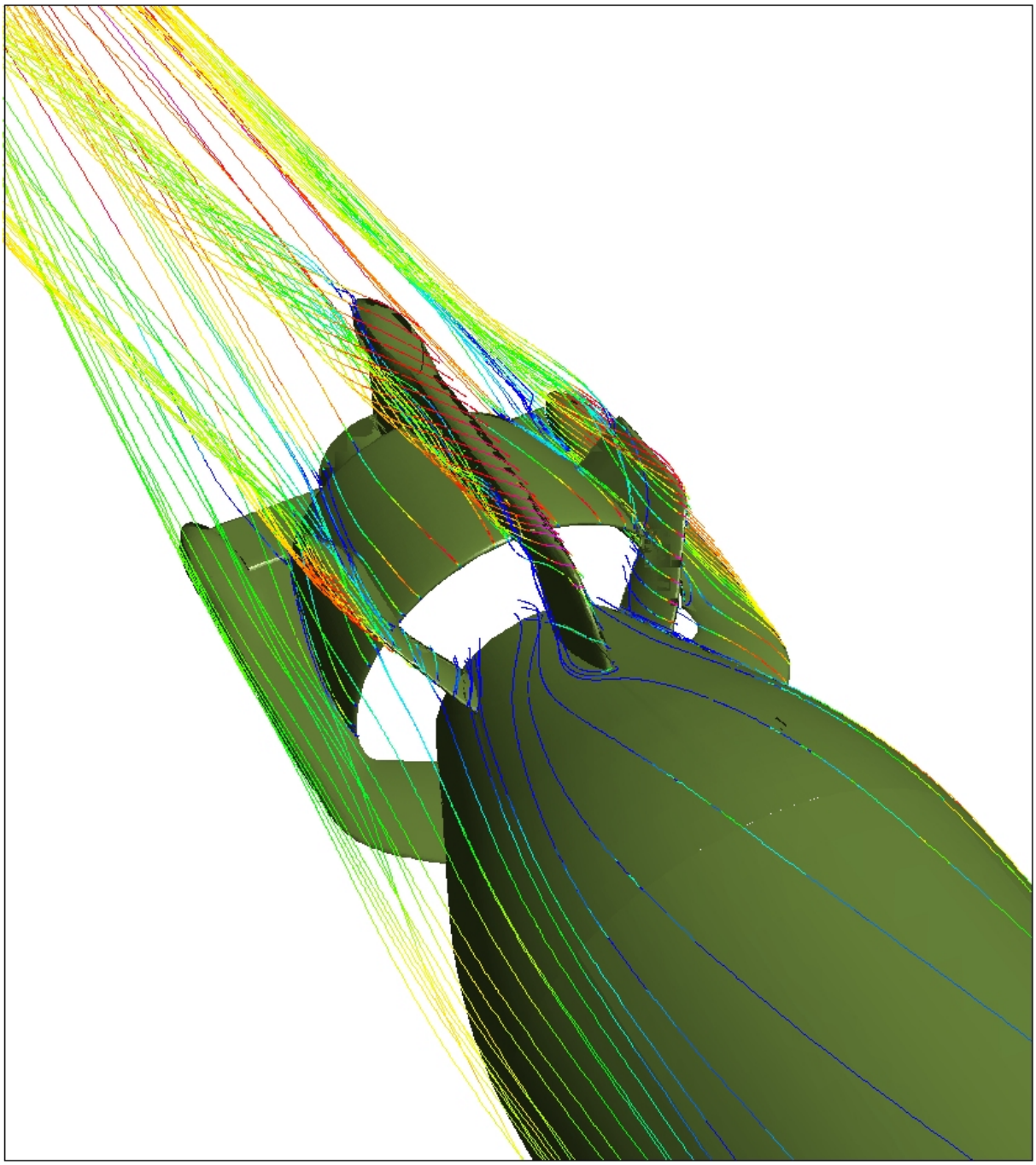

Figure 6: Flow around duct and control surfaces of underwater weapon at yaw.

Figure 7 shows cross-flow velocity vectors in planes at four axial locations around the after-body of th vehicle. The indicate the location of the vortex generated due to the yawed flow over the body. At this angle of yaw, the centre of the vortex lies well outboard of the propulsor duct, which lies near the 93% length plane. The in-flow to the propulsor causes the body vortex to pass nearer the tail of the vehicle than would otherwise be the case. The modified flow-field affects the forces experienced during manoeuvres.

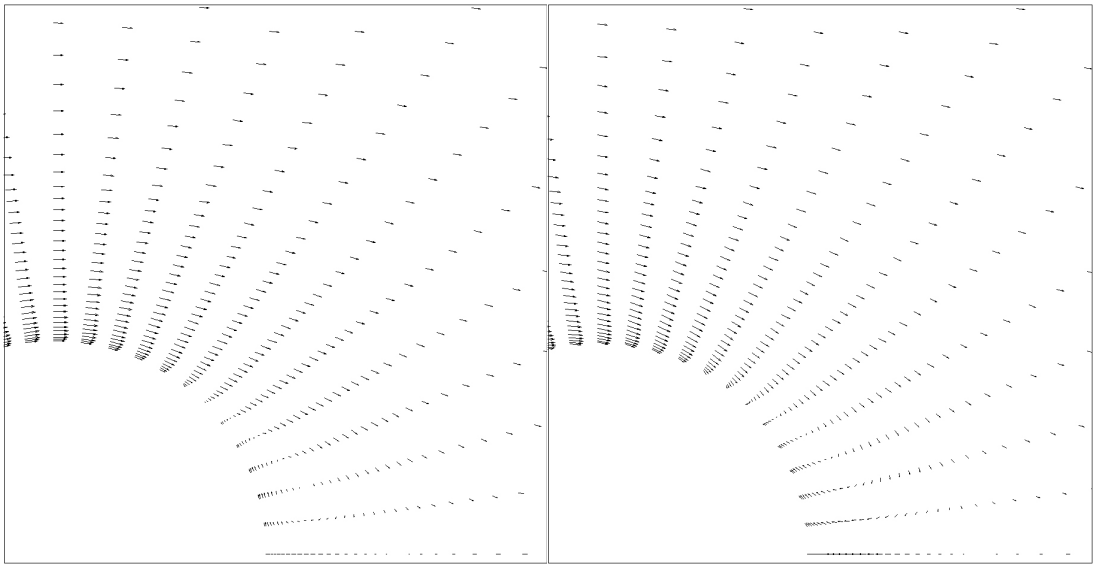

75% length 85% length

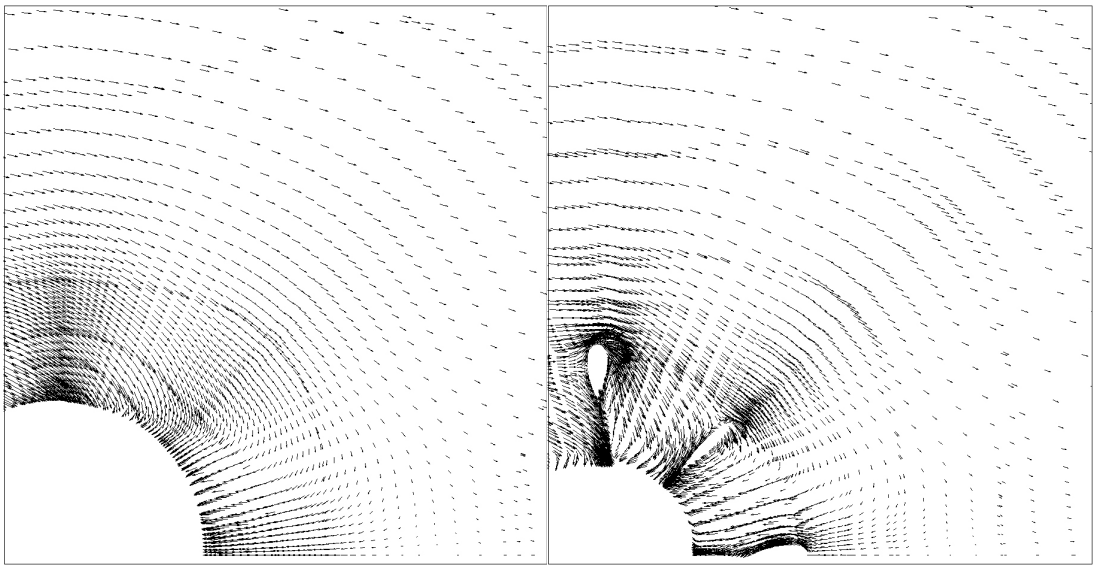

90% length 93% length

Figure 7: Flow vectors at four axial stations, 10 degrees yaw.

Overall results of side force and yawing moment coefficient from the two calculations are shown in figure 8. Test data from wind tunnel tests[3] have also been plotted for the yaw angle range of -10^o to10^o. Since the geometry is symmetrical the calculated results have been plotted for both positive and negative yaw angle, with the sign of the coefficient changed.

The measured forces show a fairly constant gradient between –5^o and 5^o followed by more non-linear behaviour beyond these angles. The CFD results predict well the gradient of yawing moment coefficient between –5^o and 5^o The non-linear behaviour, however, is over-predicted in the side force coefficient and under-predicted for the yawing moment coefficient.

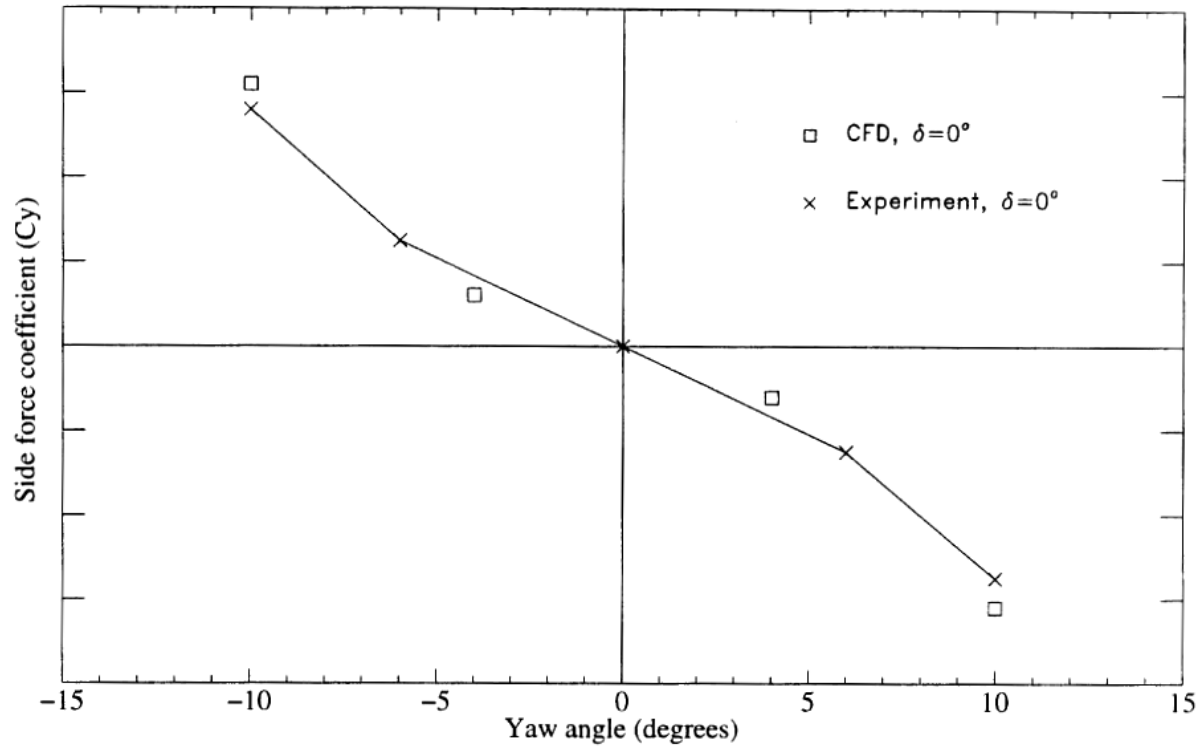

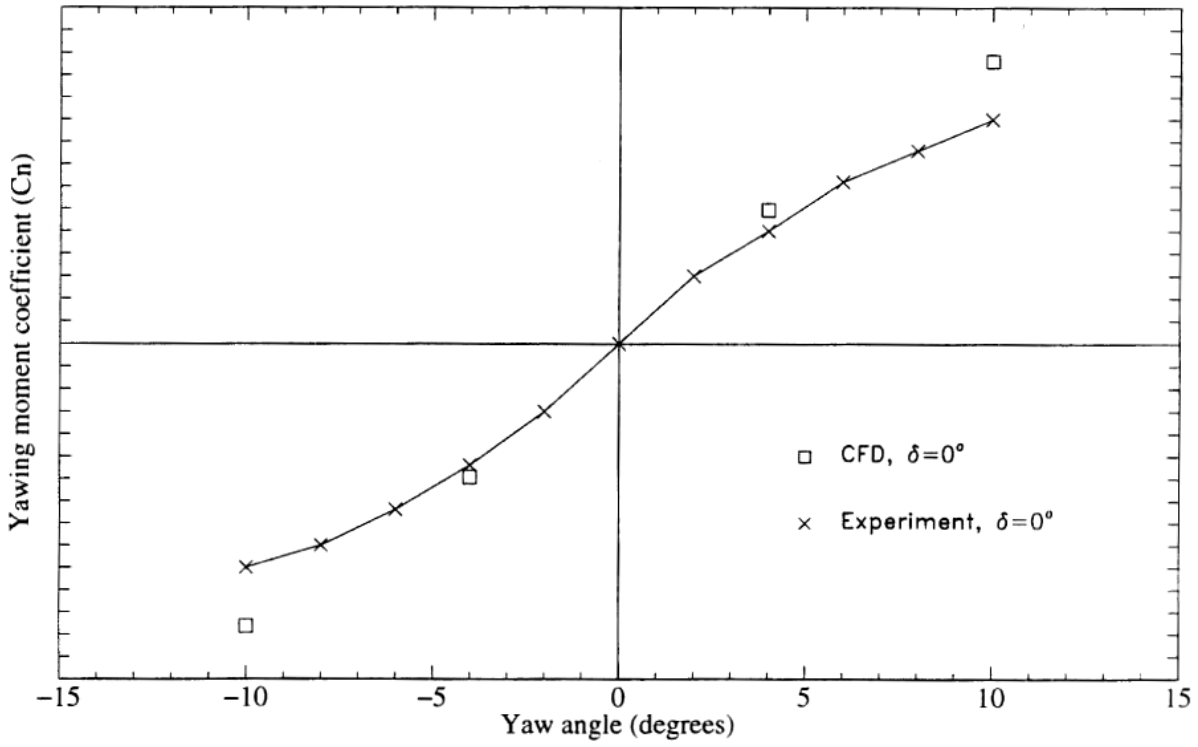

Figure 8: Effect of yaw angle on side force and yawing moment coefficient..

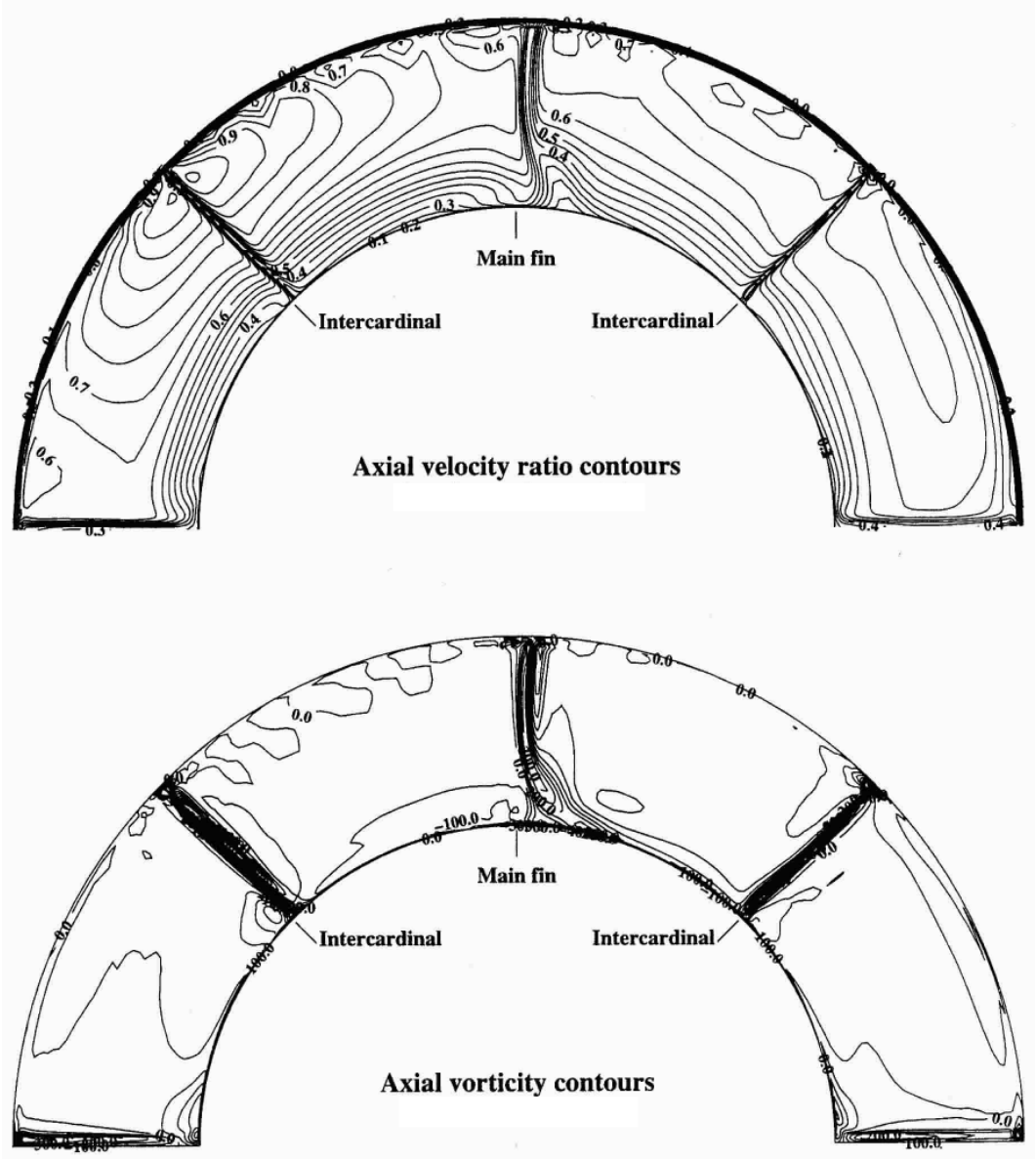

Figure 9: Propulsor in-flow at four degrees yaw angle.

At a yaw angle of 4^{o} the main-fin wake is deflected to the right and thickens, especially near the hub. This is due to the hydrodynamic loading on the fin and the associated flow deviation. An end-wall corner loss region has developed due to the cross passage pressure gradient set-up by the loaded fin. This draws boundary layer fluid off the hub and up onto the fin suction surface. This increases the effect of the horseshoe vortex filament on the suction side of the main-fin. The increased vorticity that this produces is clear by comparing figures 4 and 9.

The axial velocity of the mid-stream flow in the left half of the passage is greater near to the duct, compared with zero yaw angle. The right hand-side exhibits a slightly thinner hub boundary layer. The left-hand intercardinal wake is slightly thicker than the right-hand wake. The wakes of the main-fins lying along the plane of symmetry are thicker, and their vorticity is increased.

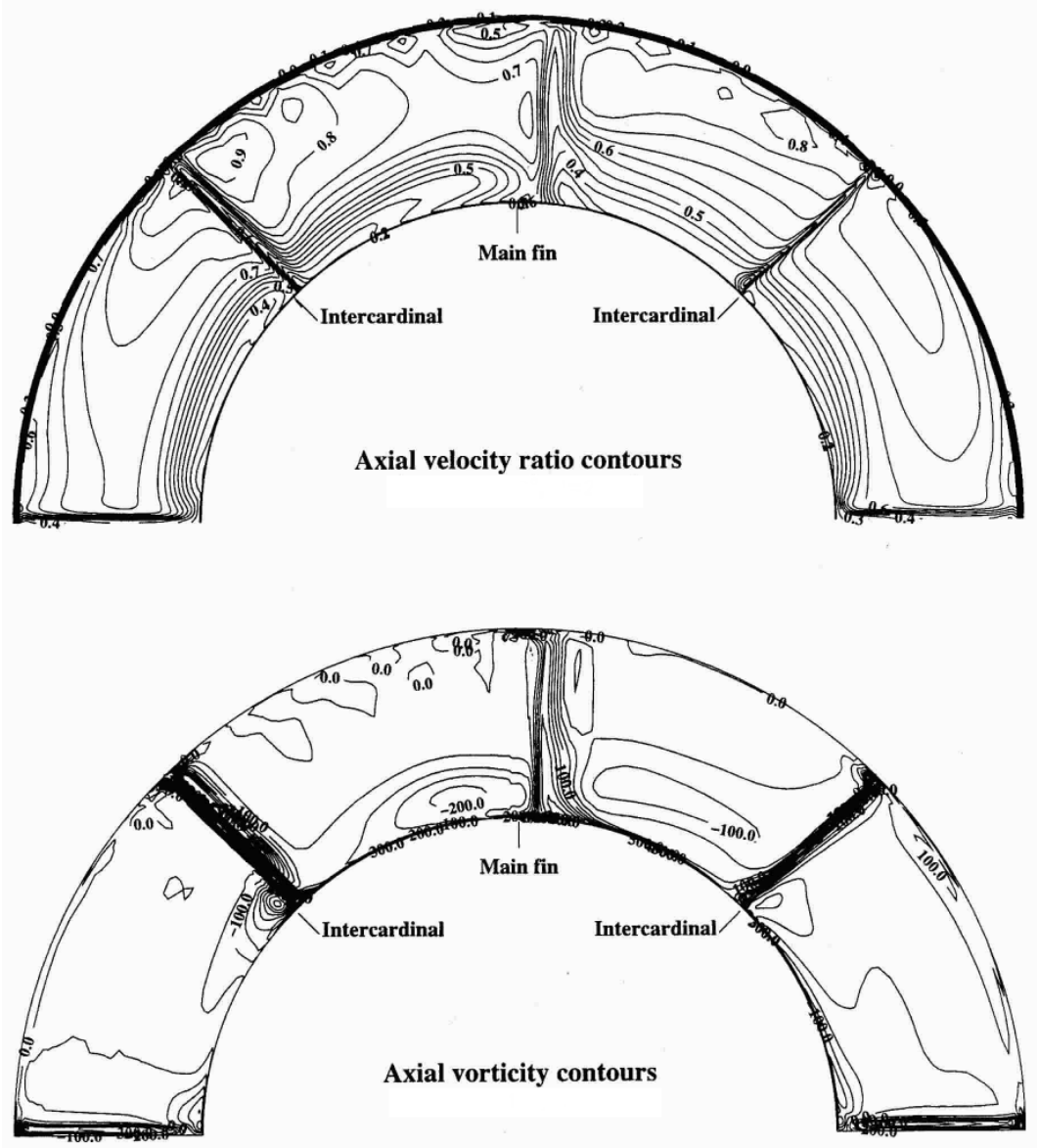

Figure 10: Propulsor in-flow at ten degrees yaw angle.

Figure 10 shows the propulsor in-flow distribution when the yaw angle is increased to 10^{o}. At this yaw angle the C_n and C_y curves start to become non-linear (figure 8) and this behaviour is apparent in the contours. Vortex cores are predicted to the left and right of the main-fin near the hub and to the left of the left-hand intercardinal fin. These are negative in sign (clockwise rotation in this view). This is evidence of boundary layer skew on the hub formed as the free-stream fluid moves from left to right above the boundary layer. A core of increased axial velocity has also formed near the duct and to the left of the main-fin. This is possibly a feature related to the geometry where the duct meets the fin. Flow has to accelerate around the underside of the fin at this junction when the body is at yaw.

Conclusions

Analysis of the flow around a fully configured underwater weapon, including duct, fins, rotor, stator and rudder has been completed using computational fluid dynamics software. Grid generation was facilitated by the use of independent blocks that are later joined together using General Grid Interfaces.

Predictions of the overall axial force, side force and moment coefficients in yawed flow showed encouraging agreement with test data, when the fluid dynamic coupling between the body, fins and propulsor were included in the CFD calculations.

The CFD results can be analysed to extract key, steady manoeuvring derivatives of the vehicle, which can be compared with measured data for validation. In this way it will be practicable to predict the stability and dynamics of future underwater weapons, in order to program operational performance simulation software, and hence predict the hydrodynamic performance of future underwater weapons with reduced need for expensive, scale-model testing.

Suggestions for further work include: additional predictions at a greater range of operating conditions, such as combinations of yaw and pitch angles. Fully unsteady calculations of the rotor and stator flows could be carried out to assess the interactions between the blade-rows and quantify the effect on manoeuvring dynamics. Calculations on different vehicle geometries, where further experimental results are available, would increase confidence in the CFD tools. For example, a pre-swirl pump-jet with forward mounted, or outboard control surfaces could be modelled and compared with the post-swirl case described here.

References

1. Lyes P. A. Application of CFD to Underwater Weapon Dynamics. Stage 1 to 3 Reports. BAE Systems Unpublished Reports, June 1999 to March 2001.

2. CFX-Tascflow User Documentation, AEA Technology, 1998.

3. Hughes P. D. L. Results of tests conducted in the Rotating Beam Channel at AMTE Teddington. HT 2781, 1983.